

1 **Everything you wanted to know about Mayaro virus but were afraid to ask:**
2 **Characterization and lifecycle of Mayaro virus in vertebrate and invertebrate cellular**
3 **backgrounds**

4

5 Sujit Pujhari^{a,b, #}, Marco Brustolin^{a,c}, Chan C. Heu^{a,d}, Ronald Smithwick^b, Mireia Larrosa
6 ^{a,e}, Susan Hafenstein^{f,g} and Jason L. Rasgon ^{a#}.

7 ^a Department of Entomology, Center for Infectious Disease Dynamics and the Huck
8 Institutes of the Life Sciences, The Pennsylvania State University, University Park, PA.

9 ^b Department of Pharmacology Physiology and Neuroscience, University of South
10 Carolina School of Medicine, Columbia, South Carolina, USA

11 ^c pharmacology, Physiology, and Neuroscience

12 ^d USDA-ARS, Maricopa, AZ, USA

13 ^e Universitat Autònoma de Barcelona, Spain.

14 ^f Department of Biochemistry and Molecular Biology, The Pennsylvania State
15 University, University Park, PA.

16 ^g Department of Medicine, The Pennsylvania State University College of Medicine,
17 Hershey, PA, USA

18 #Address of correspondence to Jason L. Rasgon (jlr54@psu.edu) and Sujit Pujhari
19 (spujhari@uscmed.sc.edu)

20 Running title: **Mayaro virus characterization**

21 **Abstract**

22 Mayaro virus (MAYV) is an emerging new world alphavirus (genus *Alphavirus*, family
23 *Togaviridae*) that causes acute multiphasic febrile illness, skin rash, polyarthritis, and
24 occasional severe clinical phenotypes. The virus lifecycle alternates between
25 invertebrate and vertebrate hosts. Here we characterize the replication features, cell
26 entry, life cycle, and virus-related cell pathology of MAYV using vertebrate and
27 invertebrate *in vitro* models. Electron dense clathrin-coated pits in infected cells, and
28 reduced viral production in the presence of dynasore, ammonium chloride, and
29 bafilomycin, indicates that viral entry occurs through pH-dependent endocytosis.
30 Increase in FITC-dextran uptake (an indicator of macropinocytosis) in MAYV-infected
31 cells, and dose-dependent infection inhibition by 5-(N-ethyl-N-isopropyl) amiloride (a
32 macropinocytosis inhibitor), indicated that macropinocytosis is an additional entry
33 mechanism of MAYV in vertebrate cells. Acutely infected vertebrate and invertebrate
34 cells formed cytoplasmic or membrane-associated extracytoplasmic replication
35 complexes. Mosquito cells showed modified hybrid cytoplasmic vesicles that supported
36 virus replication, nucleocapsid production, and maturation. Mature virus particles were
37 released from cells by both exocytosis and budding from the cell membrane. MAYV
38 replication was cytopathic and associated with induction of apoptosis by the intrinsic
39 pathway, and later by the extrinsic pathway in infected vertebrate cells. Given that
40 MAYV is expanding its geographical existence as a potential public health problem, this
41 study lays the foundation of biological understanding valuable for therapeutic and
42 preventive interventions.

43 **Keywords:** Arbovirus, Mayaro virus, macropinocytosis, cytopathic vacuoles, virus-host
44 interactions.

45

46

47

48

49

50

51

52

53

54

55

56

57

58

59

60

61

62 **Introduction**

63 Mayaro virus (MAYV) is a neglected emerging arboviral pathogen. It was first isolated in
64 1954 from Trinidad and Tobago, and since then, outbreaks have been reported in South
65 and Central America [1]. Many of its clinical features, including arthralgia, overlap with
66 Dengue and Chikungunya; however, biphasic or intermittent hyperthermia can
67 distinguish MAYV from other arboviral infections [2, 3]. MAYV can cause neurological
68 complications, myocarditis, hemorrhagic manifestations, and death [2, 4]. MAYV
69 alternates between vertebrate and invertebrate hosts and is primarily transmitted
70 through the bite of female *Haemagogus* (in sylvatic cycle) and *Aedes* (urban and peri-
71 urban cycle) mosquito species in South and Central America [5-7]. Transmission by
72 multiple *Anopheline* mosquito species has also been demonstrated through laboratory
73 studies, indicating a potential risk of this emerging virus in other parts of the world [8]
74 (Fig.1).

75 MAYV is a positive-sense, single-stranded-RNA virus that belongs to the genus
76 *Alphavirus* in the family *Togaviridae*. It is a member of the Semliki Forest virus antigenic
77 complex that consists of eight other viruses: Semliki Forest, Chikungunya (CHIKV),
78 Bebaru, Getah, Ross River (RRV), O'nyong-nyong (ONNV), Sagiyma and Una viruses
79 [9]. Its genome is approximately 11.7 kb and encodes four nonstructural proteins (nsP1-
80 4), six structural proteins (capsid [C], envelope [E] proteins [E3, E2, E1], 6K, and trans-
81 frame), and two open reading frames (ORFs) [10]. Based on its whole-genome
82 phylogeny, MAYV has three genotypes (D, L, and N) which are highly conserved with
83 approximately 17% nucleotide divergence across all three genotypes, and 4% among D
84 strains. It is thought that genotypes D and L diverged approximately 150 years ago, and

85 genotype N diverged approximately 250 years ago [11]. Genotype D has a diverse
86 distribution in South America and the Caribbean, genotype L was detected in certain
87 parts of Brazil whereas N genotype was found only in a localized region in Peru [12].
88 The ability of MAYV to recombine with other strains and related viruses may arise in
89 new lineages [32].

90 Most of our understanding of the cellular and molecular biology of MAYV is based on
91 studies with other alphaviruses. To bridge this critical knowledge gap on the biology of
92 this emerging yet neglected arthritis-causing alphavirus, we used mosquito and
93 vertebrate cells to characterize its biology. This study provides a comprehensive
94 investigation on the lifecycle of MAYV, its replication characteristics, and cellular tropism
95 to provide insight into the interaction of MAYV with its mosquito and vertebrate host.
96 Given that MAYV is expanding its geographical existence as a potential public health
97 problem, this study will lay down the foundation of biological understanding valuable for
98 therapeutic and preventive interventions.

99

100 **Materials and Methods**

101 **Cell culture**

102 C6/36 (*Aedes albopictus*) cells, Aag2 (*Aedes aegypti*), and Sua5b (*Anopheles gambiae*)
103 cells were maintained in Schneider's insect cell culture medium. Vero (African green
104 monkey kidney), BHK-21 (Baby Hamster Kidney), and Huh7.5 (Human liver) cells were
105 maintained in Dulbecco's modified Eagle's medium (DMEM) supplemented with 10%
106 fetal bovine serum (FBS), 50 units ml⁻¹ of penicillin and 50 µg ml⁻¹ of streptomycin.

107 Vertebrate cells were cultured in a 37 °C incubator with 5% CO₂, while invertebrate
108 (mosquito) cells were cultured at 28 °C incubator without CO₂.

109

110 **Antibodies**

111 CHIK-48, anti-E2 protein (BEI resources, USA); anti-dsRNA, dsRNAJ2 (SCICONS,
112 Hungary); Cleaved caspase-3, 9664, (Cell Signaling Technology [CST], USA); Cleaved
113 Caspase-9, 52873 (CST, USA); Caspase-8, SAB3500404 (Sigma, USA); PARP,
114 9542 (CST, USA); HSP60, SAB4501464 (Sigma, USA); Phalloidin-594; actin
115 (Invitrogen, USA).

116

117 **Viral growth kinetics by focus forming assay (FFA)**

118 Approximately 3 × 10⁴ Vero cells per well were seeded in a 96-well plate and incubated
119 overnight. Virus samples (BeAn 343102, D strain of MAYV) were diluted in ten-fold
120 serial dilutions in DMEM without FBS supplemented with antibiotics; 30 µl from each
121 dilution was added to each well containing the cells and incubated at 37°C. One hour
122 post infection, 100 µl of overlay media (1X DMEM medium, 10% FBS, 50 units ml⁻¹
123 penicillin, 50 µg ml⁻¹ streptomycin, 1% carboxymethyl cellulose) was added. Twenty-
124 four hours post-infection, the overlay was removed; to fix the cells, 100 µl of 4%
125 paraformaldehyde in phosphate buffered saline (PBS) was added and incubated at RT
126 for 15 minutes. For antibody probing, the plate was first blocked for 30 minutes at RT
127 with 50 µl of blocking solution (3% BSA, 0.25% triton x in PBS), followed by the addition
128 of 30 µl of primary antibody (CHIK-48, anti-E2 protein) for 2 h at RT or overnight at 4°C.

129 Plates were then washed three times with PBS. Secondary antibody (Alexa 488 Goat
130 anti-Mouse, ThermoScientific) was added (30 μ l per well) and incubated for 1 h at RT.
131 Plates were washed three times with distilled water, air-dried and screened manually
132 under 4x objective of Olympus microscope. Viral titers were expressed as FFU ml $^{-1}$.

133

134 **Heat treatment of virus particles**

135 Approximately 10^6 FFU of MAYV, Sindbis virus (SINV) and O'nyong yong virus (ONNV)
136 were subjected to a thermal gradient treatment from 30 to 60 °C for 3 h with a
137 thermocycler (Bio-Rad T100 Thermal Cycler), after which samples were immediately
138 titrated on Vero cells. A non-heat-treated virus control kept at 4°C for 3 h was also
139 included. The ratio of the number of FFU in heat-treated versus the non-heat-treated
140 viruses was calculated to determine the relative infectivity.

141

142 **Plaque assay**

143 Vero cells (5×10^5 cells/well) were grown overnight to a confluent monolayer in 6 well
144 plates and infected with serial dilutions of MAYV or ONNV or SINV-infected culture
145 supernatant. Virions were allowed to adsorb on the cell surface for 1 hour at 37°C with
146 5% CO₂; subsequently, monolayers were rinsed with DMEM without FBS, and overlay
147 medium (1% methylcellulose in DMEM with 5% FBS) was added. The plates were
148 incubated at 37 °C in a 5% CO₂ incubator for 72 h. At the end of the incubation period,
149 overlay media was removed and fixed with 1 ml of 4% PFA solution at RT for 15
150 minutes. After one washing with PBS, methylene blue prepared in methanol was added

151 onto the fixed cells. After 30 minutes of incubation, plates were cleaned in tap water,
152 and plaques size were measured.

153

154 **Effect of lysosomotropic drugs on MAYV entry**

155 BHK-21 (3×10^4 cells/well), Huh7.5, and C6/36 (5×10^4 cells/well) cells were seeded in
156 96 well plates the day before treatment. Cells were pretreated for 3h in serum-free
157 media containing ammonium chloride or bafilomycin A1 (see Results for concentrations
158 used). Following incubation, cells were infected with MAYV at an MOI of 1 in the
159 presence of each compound for 1h at 37°C. Cells were washed, complete media
160 containing each compound was added, and were incubated at 37°C for 16h.
161 Additionally, no drug and drug with no virus control were included. After incubation, cells
162 were fixed with 4% PFA, permeabilized, processed for immunofluorescence using virus-
163 specific antibodies, and virus-positive cells were quantified.

164

165 **Immunofluorescence analysis of infected cells**

166 Huh7.5 or C6/36 cells were seeded in two well chamber slides at a density of 2×10^5
167 cells per well. Cells were then infected with MAYV at an MOI of 1 or mock-infected and
168 incubated at 37 °C (Huh7.5) or 28 °C (C6/36). After 1 h, cells were washed with DMEM
169 or Schneider's insect cell culture medium without FBS and replaced with fresh growth
170 medium and then incubated at 37 °C (Huh7.5) or 28 °C (C6/36). Cells were fixed with
171 4% PFA for 15 minutes at RT at 12hpi for detection of dsRNA or at 24hpi for E2 protein
172 detection. Cells were then blocked with 500µl of blocking solution (3% BSA with 0.25%

173 Triton-X in PBS) for 30 min. at room temperature before incubation with CHIK-48 (anti-
174 E2) (1:500) or dsRNA antibody (1:100) diluted in blocking buffer overnight. Next day
175 cells were washed three times with PBS/T and incubated with Alexa Fluor 488 or 595
176 secondary antibodies (Life Technologies) diluted in PBS/T for 1 h at RT. After
177 incubation, cells were washed three times with PBS/T. Finally, for nuclear staining, cells
178 were incubated with 500 ul of PBS with Hoechst stain for 2 minutes, followed by a final
179 washing with distilled water. Cells were mounted using 1.5mm cover glass with ProLong
180 Diamond Antifade Mountant (Life Technologies). Images were taken using a Zeiss LSM
181 800 confocal microscope.

182

183 **TEM of infected cells**

184 Cell pellets were fixed in 3% glutaraldehyde in PBS for 1 h at room temperature,
185 washed with 0.1 M cacodylate buffer, and incubated in 1% OsO₄ (in 0.1 M cacodylate
186 buffer) for 40 min at room temperature. Samples were then washed once with 0.1 M
187 cacodylate buffer and once in 80% acetone for a further incubation overnight at 4 °C in
188 2% uranyl acetate/80% acetone. The following day, serial dehydration and resin
189 infiltration steps were performed as follows: 2 × 10 min with 80% acetone, 2 × 10 min
190 with 90% acetone, 3 × 20 min with 100% acetone, 1 × 90 min with 50% Epon/50%
191 acetone, 1 × 90 min with 75% Epon/25% acetone and 1 × 90 min with 100% Epon.
192 Epon was replaced by fresh 100% Epon with polymerization accelerator BDMA and
193 embedded at 65 °C for 72 h. Resin blocks were sectioned using a DiATOME Ultra
194 Diamond Knife on a Leica EM UC7 ultramicrotome, from which 50nm sections were
195 obtained and mounted on EM copper grids with carbon coating. Sections were post-

196 stained in 2% uranyl acetate in water and Reynolds' lead citrate for 1 min each and then
197 processed for TEM imaging using a FEI Tecnai F20 S/TEM electron microscope.

198

199 **Cell cytotoxicity and viability assay**

200 Neutral red uptake assay was used to evaluate MAYV-induced cell cytotoxicity/death
201 and cytotoxicity of chemicals in Huh7.5 cells. In brief, Huh7.5 cells were seeded into 96-
202 well plates at a density of 2.5×10^4 cells per well and allowed to attach for 12 h. The
203 outer perimeter wells of the plate were left blank as they often have decreased cell
204 growth. Cells were infected with 0.1 or 1 MOI of MAYV at different time points in order
205 to harvest the plates at 3, 6, 12, 24, 36, and 48 h of post-infection. Cell plates were
206 washed once and replenished with 100ul of neutral red medium (40 ug ml^{-1}) which was
207 prepared a day before and incubated at 37°C. After 2 h of incubation at 37 degree,
208 plates were washed (with PBS) and 150 ul of neutral red destain solution (56% ethanol
209 [96% concentration], 49% deionized water, 1% glacial acetic acid) was added to each
210 well. To extract the neutral red from the cells, plates were agitated for 10 minutes on a
211 microtiter plate shaker. The optical density of the plates was measured at 540 nm in a
212 microtiter plate reader spectrophotometer. Each plate had blanks that contained no cells
213 and cells without virus as no treatment reference. Cell cytotoxicity was measured using
214 the following formula % viable cells = $(\text{Abs}_{\text{samp}} - \text{Abs}_{\text{blank}}) / (\text{Abs}_{\text{control}} - \text{Abs}_{\text{blank}}) \times 100$.

215

216 **Western blot**

217 MAYV infected and mock infected cells were harvested at the time points stated above
218 by a cell scraper and pelleted by centrifugation. Cell pellets were washed twice with
219 PBS and lysed in RIPA buffer (20 minutes on ice) with protease inhibitor cocktail. The
220 lysate was cleared by centrifugation at 14,000 rpm for 20 min at 4°C and resolved on
221 10% or 12% sodium dodecyl sulfate polyacrylamide gel electrophoresis (SDS/PAGE).
222 Proteins were transferred to nitrocellulose membranes (0.45, Bio-Rad). Membranes
223 were blocked in 5% milk in TBS-tween 20 (50 mM Tris-HCl pH 7.4, 250 mM NaCl, 0.1%
224 Tween-20) for 1 hour. Membranes were probed with primary antibody overnight at 4°C,
225 then with corresponding HRP-conjugated secondary antibodies in 5% milk/TBS-tween.
226 Signals were detected with the enhanced chemiluminescence method (GE healthcare).

227

228 **Infection Center assay**

229 At 6hpi Huh7.5 cells were washed, suspended with the aid of trypsin, centrifuged, and
230 resuspended in DMEM supplemented with ZVAD-FMK or DMSO. The infected cells
231 were counted and diluted. Then 0.03 ml of the infected cell dilution was added onto the
232 Vero cell monolayer prepared on the 96 well culture plate. To permit the infected cells to
233 settle down on the Vero cells, the medium was removed after 2 hours of incubation, and
234 100ul of methylcellulose overlay supplemented with ZVAD-FMK or DMSO was added.
235 At 24hpi, cells were fixed and processed as described for focus forming assay and
236 pictured using an epifluorescence microscope. The diameters of the foci were
237 measured using ImageJ with arbitrary units.

238

239 **Results**

240 **Growth kinetics of MAYV in vertebrate and invertebrate cells**

241 To determine the *in vitro* host range, growth kinetics, production of infectious viral
242 particles, and cytopathology of MAYV, single- and multi-step growth curve analyses
243 were performed in mammalian and insect cells (Fig. 2A). The low MOI (0.1) growth
244 curve demonstrates the release of infectious viruses in two bursts. The first burst
245 appears between 6-12 hours post-infection (hpi) in mammalian cells and after 12hpi in
246 mosquito cells. The second burst appears approximately at 24hpi in Vero and BHK-21
247 cell and after 30hpi for Huh 7.5 and mosquito cells. It is also important to note that,
248 except for BHK-21, other vertebrate and invertebrate cells showed a distinctive latent,
249 exponential, and plateau phase.

250 In all tested cell lines, MAYV replicated to high titers ($>10^7$ FFU/mL) with the exception
251 of the Aag2 cell line (from *Aedes aegypti*) where the maximum titer was 10^6 FFU/ml.
252 BHK-21 produced almost 1.5-log higher viral titer in comparison to other mammalian
253 cells, and Sua5b produced more than 2-log higher virus titer at 24hpi and 48hpi. All
254 mammalian cells caused cytopathic effects detectable after 12hpi which was
255 characterized by cell rounding and detachment. Conversely, no obvious cytopathic
256 effect was detected in mosquito cell lines.

257

258 **Physical characterization of MAYV**

259 To understand and compare the thermal stability of MAYV to other alphaviruses such as
260 SINV and ONNV, heat inactivation kinetics under different temperature conditions was

261 investigated. Viral particles produced in Vero cells were treated at temperatures ranging
262 from 25 to 55 °C for 3h, and virus infectivity was determined by focus forming assay.
263 MAYV displayed higher thermal stability at 50°C compared to ONNV, but was lower
264 than SINV (Fig. 2B). After 3h of incubation at 55°C all viruses were completely
265 inactivated.

266 Plaque size is a measure of viral replication efficiency and genetic heterogeneity among
267 the virus population. MAYV plaque morphology was examined in Vero cells at 72hpi
268 and compared to ONNV and SINV plaques. MAYV formed large (~0.8mm) and small
269 (~0.5 mm) plaques, while the other alphaviruses had only one type of plaque diameter
270 (small for SINV and large for ONNV) (Fig. 2C). The large MAYV plaques were
271 morphologically similar to ONNV, with a distinct and prominent outline. Conversely,
272 SINV plaques were smaller, hazily outlined, and less prominent.

273

274 **pH-dependent receptor-mediated endocytic entry of MAYV**

275 Electron dense cup-shaped structures (or pits) are prominent features during the entry
276 phase of MAYV, as seen in electron micrographs (see below, Fig.6i, 7i). In the receptor
277 mediated endocytosis (RME) process, these pits eventually mature and form the early
278 endosome. At a later stage, entry features a pH-dependent fusion of the viral envelope
279 with the endocytic vesicle and release of the viral genome into the cytoplasm.

280 To assess the role of RME in the entry of MAYV, we used dynasore, a pharmacological
281 dynamin GTPase inhibitor. Dynamin is a GTPase essential for pinching off of the
282 endosomes from the cytoplasmic membrane. Vertebrate and invertebrate cells were

283 pretreated (1h pre-infection) with dynasore and infected with MAYV. MAYV
284 internalization was significantly inhibited by dynasore pretreatment and its presence in a
285 dose-dependent manner indicating the role of RME in the MAYV entry process (Fig. 2D,
286 E).

287 Further, to test whether the release of MAYV into the host cytoplasm upon entry is pH-
288 dependent, we evaluated the effect of two known pharmacological inhibitors:
289 Ammonium chloride and Bafilomycin. The former is a weak base and a lysosomotropic
290 agent because of its propensity to accumulate in lysosomes, and the latter blocks the v
291 type ATPase and alters the late endosomal vesicles' pH. Pretreatment of cells (1h pre-
292 infection) and maintaining the chemicals in the culture medium with increasing
293 concentrations revealed a significant dose-dependent reduction in virus particle
294 production (Fig. 2D, E).

295

296 **Spatial distribution of viral replication complex and viral particles**

297 To demonstrate the intracellular spatial distribution pattern of the viral replication
298 complex, Huh-7.5 and C6/36 cells were infected with MAYV and assayed with dsRNA
299 antibodies 6hpi. dsRNA is an intermediate in the replication complex of RNA viruses
300 which was found to be distributed throughout the cytoplasmic compartment of both cell
301 lines but absent in the filopodial extensions (detected using phalloidin) (Fig. 3A). Z-stack
302 3D analysis revealed that replication units (dsRNA puncta) were distributed both in
303 cytoplasm and cell membrane indicated by the distribution of dsRNA puncta both in and
304 above the plane of the nucleus (Fig. 3B, C). This corroborates with the distribution of

305 replication vesicles both in the cytoplasm and plasma membrane (Fig. 3D), as seen
306 under TEM (described below).

307 To detect the induction of filopodial nanofiber-like extensions in MAYV infected cells and
308 its ability to infect neighboring cells, a confocal immunofluorescence analysis was
309 performed. Phalloidin and a CHIKV cross-reactive antibody were used to detect F-actin
310 and MAYV E2 glycoprotein, respectively, in Huh-7.5, and C6/36 mosquito cell lines
311 24hpi MAYV infection. Both cell types exhibited nanofiber-like extensions connecting
312 neighboring cells with a high density of viral particles at the surface of the membrane
313 (Fig. 4, extreme right panel). MAYV E2 glycoproteins were primarily localized at the cell
314 membrane and throughout the cytoplasm. Nevertheless, partial co-localization between
315 E2 and actin was found in discrete areas (Fig. 4). This indicates that MAYV may
316 transmit from cell-to-cell via filopodia.

317

318 **MAYV utilizes macropinocytosis for its entry**

319 Filopodial cup-like extensions engulfing virus particles were spotted during the
320 ultrastructural study in Huh7.5, BHK-21, and C6/36 cells, suggesting a process of
321 macropinocytosis (Fig. 5A). To assess the involvement of macropinocytosis in MAYV
322 entry, a functional fluid uptake assay was performed. Both vertebrate (BHK-21 and Huh-
323 7.5) and invertebrate (C6/36 and Aag2) cell lines were incubated with 1uM FITC-
324 dextran, and intake of FITC labeled dextran evaluated by detection of fluorescence
325 signal in the presence or absence of MAYV. An increased FITC-dextran uptake was

326 noted in vertebrate cells infected with MAYV, but no changes were detected in mosquito
327 cells (Fig. 5B).

328 For further validation, a quantitative MAYV infection assay was performed in the
329 presence of EIPA, a pharmacological inhibitor of macropinocytosis that inhibits Na^+/H^+
330 exchange. A dose-dependent reduction in infection in both BHK-21 and Huh-7.5 cells
331 was observed, but not was not observed in mosquito cells, reinforcing the role of
332 macropinocytosis as an important entry pathway of MAYV in vertebrate cells (Fig. 5C).

333

334 **Ultrastructural analysis of Huh7.5 and C6/36 cells infected with MAYV**

335 To provide ultrastructural details, thin-section transmission electron microscopy of
336 Huh7.5 and C6/36 cells infected with MAYV was performed (Fig. 6). In Huh7.5 cells, it
337 was observed that MAYV replicated (Fig. 3D) in replication spherules, matured in the
338 cytoplasmic vesicles (CPV) and egressed by both budding and exocytosis. The inner
339 membrane of CPV-I, prominent in the BHK-21 MAYV infected cells, associated with
340 bulb-shaped spherules, corresponds to the invaginations of the vacuole membranes.
341 Inside the spherule, a central dense mass of possibly replicating viral RNA was often
342 seen with a narrow neck connected it to the cytoplasm (Fig. 6iii). Spherules protruding
343 toward extracellular space were also observed (Fig. 3D). Nucleocapsids (NCs) are
344 associated with type II cytoplasmic vesicles (CPV-II) containing multivesicular
345 inclusions, amorphous material, and occasional intact-looking virions (Fig. 6iv). Different
346 types of CPV-II were seen coupled with NCs on the cytoplasmic side of the vacuole
347 and/or the interior of the double-membrane CPV-II. CPV-I and CPV-II were both present

348 in the infected cells 6hpi, though CPV-II was more abundant at 12hpi. Release of
349 matured viral particles by budding from PM as well as through exocytosis were evident
350 on the TEM micrographs (Fig.6 v,vi).

351 In C6/36 cells, viral entry through RME was seen (Fig. 7i). Furthermore, similar to the
352 infection of Huh7.5 cells, replication spherules (Fig. 3D), NC-containing vesicles,
353 budding virus, and exocytic vesicles carrying mature viral particles were detected in the
354 infected mosquito cells. In contrast to the series of membrane-attached spherules facing
355 inside the CPV-I of BHK-21 cells, in C6/36 cells, most of the clustered spherules were
356 unattached to the vesicular membrane (Fig. 7ii, iii). NCs were also observed inside and
357 nearby the CVP-II membrane (Fig. 7iv), demonstrating that MAYV maturation and
358 replication occur in the same cellular space. Intermediary CPV-I and CPV-II replication
359 spherules and internally budded viral particles were observed in both early and late
360 phases of infection (Fig. 7ii, v) . These modified membrane structures were also seen
361 near the rough endoplasmic reticulum and Golgi complexes. Furthermore, NCs close to
362 the PM for budding and internally budded mature viral particles inside secretory
363 intraluminal vesicles were seen (Fig. 7vi, vii).

364

365 **MAYV induces both mitochondrial dependent and independent apoptosis**

366 MAYV replication in Vero, BHK-21, and Huh-7.5 cells resulted in cytopathological
367 changes characterized by cellular fusion and multinucleated giant syncytia, detachment
368 of infected cells, and eventually cell lysis and death. To assess the involvement of

369 MAYV in the apoptosis pathway (Huh7.5 cells), a cell viability test, and a PARP and
370 Caspase detection study were performed.

371 Cell viability of MAYV infected Huh-7.5 cells was quantitatively measured through
372 neutral red uptake assay. Neutral red is a eurhodin dye, actively transported into live
373 cells, which stains lysosomes and is subsequently measured to determine cell viability.

374 Cell viability was reduced up to ~40% at 24hpi and more than 90% at 48hpi (Fig. 8A). A
375 series of morphological changes, including cytoplasmic blebbing, mitochondrial
376 swelling, chromatin condensation, and nuclear fragmentation, were observed in the
377 ultrastructural analysis of MAYV infected cells (Fig. 8B).

378 Poly (ADP-ribose) polymerase (PARP) is an enzyme that suppresses nuclear
379 fragmentation and apoptotic body formation. Under cellular stress such as viral
380 infection, PARP is cleaved and compromises the cellular viability. Cleaved PARP, a
381 marker of cells undergoing apoptosis, is detected at 12hpi and notably at its peak at
382 24hpi in the immunoblot of cells infected with MAYV. Additionally, stained cells with
383 Hoechst 33342 revealed that MAYV induced chromatin condensation, nuclear
384 fragmentation at 12hpi and is extensive around 36hpi, correlating with the PARP
385 immunoblot results (Fig. 8C lower panel). Caspase-3, a cysteine protease, activates the
386 PARP enzyme. Cleaved caspase-3 which is the active form of caspase-3 was detected
387 at 36 and 48hpi (Fig. 8C upper panel) in the MAYV infected Huh7.5 cell lysates.

388 Caspase-9, an intrinsic pathway marker, and caspase-8, which initiates the extrinsic
389 pathway, were detected in MAYV infected cells through immunostaining at 12hpi and
390 24hpi, respectively. Furthermore, active caspase-3, which cleaves the PARP enzyme
391 and culminates in nuclear fragmentation and cell death, was detected at 12hpi in the

392 immunoblot. This suggests that apoptosis which is led by the extrinsic pathway due to
393 MAYV infection is subsequent to the early intrinsic pathway (Fig. 8D).

394 Finally, to test the hypothesis that MAYV utilizes the apoptosis pathway to maximize its
395 spread, a co-culture experiment was designed. MAYV Huh7.5 infected cells pretreated
396 with caspase inhibitor (ZVAD-FMK) were co-cultured with Vero cells that served as the
397 infection center. The focus size formed by the caspase inhibitor treated cells was
398 reduced up to 50% compared to the control group indicating that MAYV utilizes the
399 apoptosis process to maximize the infection process (Fig. 8E).

400

401 **Discussion**

402 Like other members of alphaviruses, the life cycle of MAYV is rapid and infectious virus
403 can be detected in the culture supernatant as early as 3-5hpi in vertebrate cells and 7-
404 9hpi in mosquito cells [13]. The viral titers are similar in mosquito and vertebrate cells
405 at 24hpi and the viral titers in supernatants reach 10^7 – 10^8 FFU/ml within 48h, depending
406 on the cell types. Further in agreement with previous reports of transmission of MAYV
407 by *Anopheles* mosquitoes [8], Sua5b, a cell line derived from *Anopheles gambiae*,
408 supported efficient replication and produced high viral titer similar to *Aedes albopictus*
409 C6/36 cells. The lower viral titer in Aag2 cells compared to other insect cells and early
410 plateau (36hpi) is not surprising, as Aag2 cells are persistently infected with insect-
411 specific viruses which may possibly interfere with replication of MAYV [14]. MAYV had
412 also been reported to replicate to high titer in avian cell lines which migratory birds has
413 been hypothesized to be its reservoir [15].

414 Serological diagnosis is critical not only for disease surveillance but also for bedside
415 diagnostics and is preferred over molecular assays especially for resource limited setup.
416 The gold standard for serological diagnosis is the plaque reduction neutralization test,
417 which demonstrates the virus-neutralizing capacity of serum samples [16]. Before any
418 tests, the serum samples are heat-inactivated for 30 minutes at 56°C to inactivate
419 complement proteins and any infectious viral particles, if there are any. Sometimes the
420 inactivation time needs to be prolonged (e.g., 60 minutes for Western equine
421 encephalitis virus and CHIKV), ensuring the sensitivity of the assays and the safety of
422 laboratory personnel [17, 18]. We tested and compared the thermal stability of MAYV
423 along with related Alphaviruses SINV and ONNV. After 3h of incubation at 45°C some
424 of the virus particles were still infective but when the temperature increased to 55°C all
425 of them lost their infectivity. The complete inactivation of MAYV could be achieved after
426 60 minutes of incubation at 55°C.

427 *In vitro* characterization of MAYV showed overt cytopathic effects in vertebrate cells,
428 which facilitated the development of a plaque assay. The viral strain used in this study
429 forms a mixture of large and small plaques with clear and sharp boundaries
430 demonstrating the presence of a swarm of viral population with different viral entry and
431 replication capacities. In contrast, mosquito cells did not show any cytopathic effect,
432 were chronically infected with MAYV, and continuously shed infectious viral particles.
433 This demonstrates that MAYV has developed a delicate balance between the
434 mammalian host and mosquito host that allows its persistent survival in nature.
435 The role of RME has been established as one on the major route of entry for
436 alphaviruses [10, 13]. As the endosome migrates closer to the nucleus, the inner

437 compartment becomes acidic. This acidification causes the glycoproteins on the virus
438 surface to undergo conformational changes and fuse with the endosomal membrane
439 and releases the viral genome into the cytoplasm [19].

440 Mxra8, an adhesion molecule primarily expressed on epithelial myeloid, and
441 mesenchymal cells, has been recently established as a receptor for CHIKV, ONNV,
442 RRV, and MAYV [20]. Electron dense clathrin-coated pits in MAYV infected cells and
443 significant reduction of viral titers both in the vertebrate and invertebrate cells upon
444 chemical inhibition of dynamin-2, a key protein required for the formation of clathrin-
445 coated pits and vesicles, suggests the role of RME in MAYV entry [21]. Further, the use
446 of NH₄Cl and Bafilomycin that alters the pH of the early and late endosomal vesicles
447 inhibited the release of the viral genome into the cytoplasm and infection process in turn
448 and production of infectious virus [22]. This indicates that the release of the MAYV
449 genome is mediated through pH-dependent RME.

450 Upon releasing viral RNA into the host cytoplasm, which has the same polarity as that
451 of cellular mRNA, it undergoes several rounds of translational events using host cellular
452 machinery generating viral polyproteins. These are further processed by cellular and
453 newly synthesized viral proteases creating the viral replication complex. The
454 nonstructural proteins of alphaviruses induce intracellular membrane remodeling that
455 results in the appearance of cytopathic vacuoles (CPVs) and has been greatly studied
456 using the SFV model. The CPVs are of two types, CPV type I (CPV-I) and CPV type II
457 (CPV-II) [23]. Double labeling of organelle and viral nonstructural proteins showed that
458 CPV-I are derivatives of late endosomes and lysosomes, while monensin treatment
459 results in accumulation of E1/E2 glycoproteins of SFV in the trans-Golgi network (TGN),

460 indicating TGN origin of CPV-II [24, 25]. The replication complexes are strategically
461 concentrated in CPV-I and replication spherule for efficient viral genome replication and
462 to escape the cellular antiviral response [26]. These replication spherules that has
463 access to the host cellular raw materials through an opening toward the cytoplasm were
464 seen either inside CPV-I or transported to the plasma membrane [27]. Both vertebrate
465 and invertebrate cells had similar spherules with a central electron-dense material,
466 possibly the MAYV replicating RNA. dsRNAs are unique to viral infected cells and are
467 the markers of replication intermediates/replication complex [28]. In the confocal image,
468 detection of dsRNA in the plane with the nucleus indicated the replication of MAYV in
469 the cytoplasmic CPV-I, which appears during the early stage of infection and above the
470 plane of the nucleus, indicating the presence of replication complex on the cell
471 membrane that is further validated in the electron micrographs. Like other alphaviruses,
472 CPV-II was the predominant vacuolar structure in the later stage of MAYV infection both
473 in Huh7.5 and C6/36 cells. Our electron micrograph analysis showed three main
474 different populations of CPV-II in Huh7.5 cells. The first population consists of numerous
475 nucleocapsids (NCs) attached to the cytoplasmic face of membranes, second has NCs
476 enclosed inside the vesicles, and the third were transporting vesicles containing E/E2
477 viral glycoproteins from the TGN to the viral budding sites on the plasma membrane. In
478 contrast to previous reports NCs were seen in the cytoplasm close to the plasma
479 membrane of infected Huh7.5 and C6/36 cells. The assembly of NCs as matured
480 viruses was observed to take place either by a budding process from the plasma
481 membrane into the extracellular space or mature inside the CPVs transported through

482 the exocytosis pathway. The C6/36 cells had additional hybrid vesicles containing both
483 replication spherules and NCs, also having vesicles with mature virus particles.

484 Arthritogenic alphaviruses, including MAYV, have been associated with inflammation of
485 the joints and often with other tissues. Inflammation and apoptosis go in parallel with
486 disease severity. Although apoptosis eliminates infected cells, viruses have evolved to
487 manipulate this cellular antiviral mechanism for maximizing the production of progeny
488 virus and their spread to maintain a prolonged and high viremia in the vertebrate host, a
489 property that is relevant especially for arboviruses for their maintenance in the natural
490 transmission cycle. CHIKV and SINV camouflage in apoptotic blebs to facilitate infection
491 of neighboring cells. Apoptotic blebs bodies are quite evident in the MAYV infected
492 cells. Most commonly, blebs are seen during apoptosis and contain part of the
493 cytoplasm (~2%) with or without organellar fragments for recycling by the phagocytic
494 cells [33, 34]. We designed a coculture-infection center assay that produced a smaller
495 diameter focus size in the presence of apoptosis inhibitor ZVAD-FMK that inhibits
496 apoptosis at an early stage, indicating the role of apoptosis in the spread of MAYV
497 infection. Up-regulation of proapoptotic proteins or down-regulation of antiapoptotic
498 proteins can alter mitochondrial membrane permeability that can promote the release of
499 cytochrome c [29]. Cytochrome c interacts with Apaf-1 and caspase-9 and forms a
500 multiprotein complex apoptosome, leading to activation of caspase-3 and then
501 apoptosis [30,31]. Increased activation of caspase 9 during MAYV infection indicates
502 the involvement of mitochondrial intrinsic pathway. Further detection of active caspase
503 8, possibly activated by secretion of cellular or virus-induced death signal by cell

504 membrane death receptors, demonstrate that the MAYV induced apoptosis is triggered
505 through both intrinsic and extrinsic pathways.

506 In conclusion, we present a comprehensive *in vitro* characterization of MAYV in both
507 vertebrate host and invertebrate mosquito vector cells. Besides pH-dependent receptor-
508 mediated endocytosis (RME) MAYV uses macropinocytosis for entry into vertebrate
509 cells. During acute infection in vertebrate cells, MAYV achieves very high titer and
510 utilizes the apoptotic pathway for efficient transmission to neighboring cells. In mosquito
511 cells, a burst in high viral titer follows continuous virus production at reduced levels,
512 indicating the evolutionary adaptation of arboviruses with their mosquito vector. Further,
513 it will be interesting to understand and identify the molecular signature(s) that makes
514 them clinically different from their close geographical ancestors.

515

516 **Acknowledgements**

517 We thank Missy Hazen for assistance with microscopy. This work was funded by NIH
518 grants R01AI150251, R01AI128201, R01AI116636, and R21AI128918, USDA Hatch
519 funds (Accession #1010032; Project #PEN04608), and a grant with the Pennsylvania
520 Department of Health using Tobacco Settlement Funds to JLR, and grant NIH
521 R21AI128918, a seed grant from The Penn State Huck Institutes of the Life Sciences,
522 and startup grant and ASPIRE grant from the University of South Carolina to SP.

523

524 **Authors Contributions**

525 Conceptualization: SP, JLR; Methodology: SP; Data Curation: SP, MB, CCH, RS, ML;
526 Funding acquisition: JLR, SP; Writing-first draft: SP; Writing-review and editing: SP,
527 JLR, SH, MB, CCH, RS and ML; Writing- finalizing MS: JLR and SP.

528

529

530

531

532

533

534

535

536

537

538

539

540

541

542

543

544

545

546

547

548 **References**

- 549 1. Anderson CR, Downs WG, Wattley GH, Ahin NW, Reese AA. Mayaro virus: a new
550 human disease agent. II. Isolation from blood of patients in Trinidad, B.W.I. *Am J
551 Trop Med Hyg.* 1957;6(6):1012-6. Epub 1957/11/01. doi: 10.4269/ajtmh.1957.6.1012.
552 PubMed PMID: 13487973.
- 553 2. Chen Z, Lang D. The effectiveness of disease management interventions on
554 health-related quality of life of patients with established arthritogenic alphavirus
555 infections: a systematic review protocol. *JBI Database Syst Rev Implement Rep*
556 2013;11:56–72. Epub 2012/12/04. PubMed PMID: 23201089.
- 557 3. Acosta-Ampudia Y, Monsalve DM, Rodriguez Y, Pacheco Y, Anaya JM, Ramirez-
558 Santana C. Mayaro: an emerging viral threat? *Emerg Microbes Infect.* 2018 7(1):163.
559 Epub 2018/09/27. doi: 10.1038/s41426-018-0163-510.1038/s41426-018-0163-5 [pii].
560 PubMed PMID: 30254258.
- 561 4. Mourao MP, Bastos Mde S, de Figueiredo RP, Gimaque JB, Galusso Edos S,
562 Kramer VM, et al. Mayaro fever in the city of Manaus, Brazil, 2007-2008. *Vector
563 Borne Zoonotic Dis.* 2012;12(1):42-6. Epub 2011/09/20. doi: 10.1089/vbz.2011.0669.
564 PubMed PMID: 21923266.
- 565 5. Smith GC, Francy DB. Laboratory studies of a Brazilian strain of *Aedes albopictus* as
566 a potential vector of Mayaro and Oropouche viruses. *J Am Mosq Control Assoc.*
567 1991;7(1):89-93. Epub 1991/03/01. PubMed PMID: 1646286.
- 568 6. Long KC, Ziegler SA, Thangamani S, Hausser NL, Kochel TJ, Higgs S, et al.
569 Experimental transmission of Mayaro virus by *Aedes aegypti*. *Am J Trop Med Hyg.*
570 2011;85(4):750-7. Epub 2011/10/07. doi: 10.4269/ajtmh.2011.11-0359. PubMed
571 PMID: 21976583; PubMed Central PMCID: PMCPMC3183788.
- 572 7. Wiggins K, Eastmond B, Alto BW. Transmission potential of Mayaro virus in Florida
573 *Aedes aegypti* and *Aedes albopictus* mosquitoes. *Med Vet Entomol.* 2018;32(4):436-
574 42. Epub 2018/07/15. doi: 10.1111/mve.12322. PubMed PMID: 30006976.
- 575 8. Brustolin M, Pujhari S, Henderson CA, Rasgon JL. Anopheles mosquitoes may drive
576 invasion and transmission of Mayaro virus across geographically diverse regions.
577 *PLoS Negl Trop Dis.* 2018;12(11):e0006895. Epub 2018/11/08. doi:

578 10.1371/journal.pntd.0006895. PubMed PMID: 30403665; PubMed Central PMCID:
579 PMCPMC6242690.

580 9. Forrester NL, Palacios G, Tesh RB, Savji N, Guzman H, Sherman M, et al. Genome-
581 scale phylogeny of the alphavirus genus suggests a marine origin. *J Virol.*
582 2012;86(5):2729-38. Epub 2011/12/23. doi: JVI.05591-11 [pii]10.1128/JVI.05591-11.
583 PubMed PMID: 22190718.

584 10. Strauss JH, Strauss EG. The alphaviruses: gene expression, replication, and
585 evolution. *Microbiol Rev.* 1994;58(3):491-562. Epub 1994/09/01. PubMed PMID:
586 7968923.

587 11. Auguste AJ, Liria J, Forrester NL, Giambalvo D, Moncada M, Long KC, et al.
588 Evolutionary and Ecological Characterization of Mayaro Virus Strains Isolated during
589 an Outbreak, Venezuela, 2010. *Emerg Infect Dis.* 2015;21(10):1742-50. Epub
590 2015/09/25. doi: 10.3201/eid2110.141660. PubMed PMID: 26401714.

591 12. Lorenz C, Freitas Ribeiro A, Chiaravalloti-Neto F. Mayaro virus distribution in South
592 America. *Acta Trop.* 2019;198:105093. Epub 2019/07/22. doi: S0001-
593 706X(19)30715-6 [pii]10.1016/j.actatropica.2019.105093. PubMed PMID: 31325416.

594 13. Marsh M, Bolzau E, Helenius A. Penetration of Semliki Forest virus from acidic
595 prelysosomal vacuoles. *Cell.* 1983;32(3):931-40. Epub 1983/03/01. doi: 0092-
596 8674(83)90078-8 [pii]10.1016/0092-8674(83)90078-8. PubMed PMID: 6831562.

597 14. Schultz, Michaela J, Frydman HM and Connor JH. Dual Insect specific virus infection
598 limits
599 Arbovirus replication in Aedes mosquito cells. *Virology* 2018;518:406-13. Epub
600 2019/11/07. doi: 10.1016/j.virol.2018.03.022. PubMed PMID: 29625404.

601 15. Henderson JR, Taylor RM. Propagation of certain arthropod-borne viruses in avian
602 and primate cell cultures. *J Immunol.* 1960;84:590-8. Epub 1960/06/01. PubMed
603 PMID: 14400990.

604 16. Figueiredo LT, Nogueira RM, Cavalcanti SM, Schatzmayr H, da Rosa AT. Study of
605 two different enzyme immunoassays for the detection of Mayaro virus antibodies.
606 Mem Inst Oswaldo Cruz. 1989;84(3):303-7. Epub 1989/07/01. doi: S0074-
607 02761989000300003 [pii]10.1590/s0074-02761989000300003. PubMed PMID:
608 2562487.

609 17.Park SL, Huang YJ, Hsu WW, Hettenbach SM, Higgs S, Vanlandingham DL. Virus-
610 specific thermostability and heat inactivation profiles of alphaviruses. *J Virol Methods*.
611 2016;234:152-5. Epub 2016/04/16. doi: S0166-0934(16)30113-6 [pii]
612 10.1016/j.jviromet.2016.04.004. PubMed PMID: 27079828.

613 18.Yue C, Teitz S, Miyabashi T, Boller K, Lewis-Ximenez LL, Baylis SA, et al.
614 Inactivation and Removal of Chikungunya Virus and Mayaro Virus from Plasma-
615 derived Medicinal Products. *Viruses*. 2019;11(3). Epub 2019/03/15. doi: v11030234
616 [pii] 10.3390/v11030234. PubMed PMID: 30866548.

617 19.Helenius A, Kartenbeck J, Simons K, Fries E. On the entry of Semliki forest virus into
618 BHK-21 cells. *J Cell Biol*. 1980;84(2):404-20. Epub 1980/02/01. doi:
619 10.1083/jcb.84.2.404. PubMed PMID: 6991511.

620 20.Zhang R, Kim AS, Fox JM, Nair S, Basore K, Klimstra WB, et al. Mxra8 is a receptor
621 for multiple arthritogenic alphaviruses. *Nature*. 2018;557(7706):570-4. Epub
622 2018/05/18. doi: 10.1038/s41586-018-0121-3. PubMed PMID: 29769725; PubMed
623 Central PMCID: PMCPMC5970976.

624 21.DeTulio L, Kirchhausen T. The clathrin endocytic pathway in viral infection. *EMBO J*.
625 1998;17(16):4585-93. Epub 1998/08/26. doi: 10.1093/emboj/17.16.4585. PubMed
626 PMID: 9707418.

627 22.Helenius A, Marsh M, White J. Inhibition of Semliki forest virus penetration by
628 lysosomotropic weak bases. *J Gen Virol*. 1982;58 Pt 1:47-61. Epub 1982/01/01. doi:
629 10.1099/0022-1317-58-1-47. PubMed PMID: 7142969.

630 23.Soonsawad P, Xing L, Milla E, Espinoza JM, Kawano M, Marko M, et al. Structural
631 evidence of glycoprotein assembly in cellular membrane compartments prior to
632 Alphavirus budding. *J Virol*. 2010;84(21):11145-51. Epub 2010/08/27. doi: JVI.00036-
633 10 [pii]10.1128/JVI.00036-10. PubMed PMID: 20739526.

634 24.Griffiths G, Simons K, Warren G, Tokuyasu KT. Immunoelectron microscopy using
635 thin, frozen sections: application to studies of the intracellular transport of Semliki
636 Forest virus spike glycoproteins. *Methods Enzymol*. 1983;96:466-85. Epub
637 1983/01/01. doi: 10.1016/s0076-6879(83)96041-x. PubMed PMID: 6656640.

638 25.Sariola M, Saraste J, Kuismanen E. Communication of post-Golgi elements with
639 early endocytic pathway: regulation of endoproteolytic cleavage of Semliki Forest

640 virus p62 precursor. *J Cell Sci.* 1995;108 (Pt 6):2465-75. Epub 1995/06/01. PubMed
641 PMID: 7673361.

642 26. Delgui LR, Colombo MI. A Novel Mechanism Underlying the Innate Immune
643 Response Induction upon Viral-Dependent Replication of Host Cell mRNA: A Mistake
644 of +sRNA Viruses' Replicases. *Front Cell Infect Microbiol.* 2017;7:5. Epub
645 2017/02/07. doi: 10.3389/fcimb.2017.00005. PubMed PMID: 28164038.

646 27. Froshauer S, Kartenbeck J, Helenius A. Alphavirus RNA replicase is located on the
647 cytoplasmic surface of endosomes and lysosomes. *J Cell Biol.* 1988;107(6 Pt
648 1):2075-86. Epub 1988/12/01. doi: 10.1083/jcb.107.6.2075. PubMed PMID: 2904446.

649 28. Pujhari S, Brustolin M, Macias VM, Nissly RH, Nomura M, Kuchipudi SV, et al. Heat
650 shock protein 70 (Hsp70) mediates Zika virus entry, replication, and egress from host
651 cells. *Emerg Microbes Infect.* 2019;8(1):8-16. Epub 2019/03/15. doi:
652 10.1101/22221751.2018.1557988. PubMed PMID: 30866755; PubMed Central
653 PMCID: PMCPMC6455116.

654 29. Garrido C, Galluzzi L, Brunet M, Puig PE, Didelot C, Kroemer G. Mechanisms of
655 cytochrome c release from mitochondria. *Cell Death Differ.* 2006;13(9):1423-33.
656 Epub 2006/05/06. doi: 4401950 [pii]10.1038/sj.cdd.4401950. PubMed PMID:
657 16676004.

658 30. Zou H, Yang R, Hao J, Wang J, Sun C, Fesik SW, et al. Regulation of the Apaf-
659 1/caspase-9 apoptosome by caspase-3 and XIAP. *J Biol Chem.* 2003;278(10):8091-
660 8. Epub 2002/12/31. doi: 10.1074/jbc.M204783200 M204783200 [pii]. PubMed PMID:
661 12506111.

662 31. Das T, Hoarau JJ, Bandjee MCJ, Maquart M, Gasque P. Multifaceted innate immune
663 responses engaged by astrocytes, microglia and resident dendritic cells against
664 Chikungunya neuroinfection. *J Gen Virol.* 2015;96(Pt 2):294-310. Epub 2014/10/30.
665 doi: 10.1099/vir.0.071175-0. PubMed PMID: 25351727.

666 32. Mavian C, Rife BD, Dollar JJ, Cella E, Ciccozzi M, Prosperi MCF, et al. Emergence
667 of recombinant Mayaro virus strains from the Amazon basin. *Sci Rep.*
668 2017;7(1):8718. Epub 2017/08/20. doi: 10.1038/s41598-017-07152-5. PubMed
669 PMID: 28821712; PubMed Central PMCID: PMCPMC5562835.

670 33. Charras GT. A short history of blebbing. *J Microsc.* 2008;231(3):466-78. Epub
671 2008/08/30. doi: 10.1111/j.1365-2818.2008.02059.x. PubMed PMID: 18755002.

672 34. Wickman G, Julian L, Olson MF. How apoptotic cells aid in the removal of their own
673 cold dead bodies. *Cell Death Differ.* 2012;19(5):735-42. Epub 2012/03/17. doi:
674 10.1038/cdd.2012.25. PubMed PMID: 22421963; PubMed Central PMCID:
675 PMCPMC3321633.

676

677

678

679

680

681

682 **Figure Legends:**

683

684 **Figure 1. Distribution of Mayaro virus in the America and global distribution of**
685 **Anopheles vectors .**

686 Distribution of D (yellow) and L (green) strains of Mayaro virus in South America and
687 geographical areas at risk of future MAYV outbreaks highlighted in blue.

688

689 **Figure 2. Growth kinetics, thermostability, plaque morphology and cellular entry**
690 **of Mayaro virus.**

691 A) Vertebrate (Huh7.5; Human, Vero; Monkey and BHK-21; Hamster) and invertebrate
692 (*Ae. albopictus*; C6/36, *Ae. aegypti*; Aag2 and *An. gambiae*; Sua5b) cells were infected
693 with MAYV at an MOI of 0.1 and 1. Culture supernatants were harvested every 2-hour
694 intervals up to 12-hour post infection, then at every 6-hour up to 36-hour post infection
695 and a final sample was harvested at 48-hour post infection. Viral titers were quantified in
696 the harvested samples using focus forming assay using Vero cells and growth curves
697 were plotted. B) Mayaro, Sindbis and O'nyong'nyong virus thermostability. Stocks of
698 indicated viruses were incubated at 4, 25, 30, 35, 40, 45, 50 and 55°C for 180 minutes
699 and the number of infectious particles determined by focus forming assay C) Known
700 titer stocks of MAYV, ONNV and SINV (15-20 PFU/100ul) were used to produce
701 plaques in 6 well plates on Vero cell monolayer as detailed in the method section. The
702 plaque diameters were measured. D and E) Effect of Dynasore, NH4Cl and Bafilomycin
703 on MAYV entry process. D) Huh7.5 and E) C6/36 cells were treated before and after
704 infection with the indicated doses of the chemicals. MAYV was adsorbed to cells at 1
705 MOI for one hour and non-adsorbed virus was removed, virus in the culture supernatant

706 were collected at 24hpi for Huh7.5 and 36hpi for C6/36 and titrated. Data from three
707 independent experiments were plotted, error bars indicate standard deviations of the
708 means.

709

710 **Figure 3. MAYV replication spherules on the plasma membrane and cytoplasmic**
711 **compartment of Huh7.5 and C6/36 cells.**

712 A) Huh7.5 (upper panel) and C6/36 (lower panel) cells were infected with 1 MOI of
713 MAYV, 6hpi cells were fixed and stained for dsRNA (green), filamentous actin (F-actin)
714 filament with phalloidin (red) and nucleus (blue) with Hoechst stain. B) z-stack analysis
715 of the distribution of dsRNA on different planes of infected cells C) Model of expected
716 distribution pattern of dsRNA (green), marker of the viral replication complex, at different
717 planes in a MAYV infected cell with respect to the nucleus. D) A) Huh7.5 and C6/36
718 cells infected with MAYV at 5 MOI processed and scanned under TEM showing bulb
719 like replication spherules on the cell surface.

720

721 **Figure 4. Cytoplasmic distribution of MAYV and cell-to-cell migration through**
722 **nanofiber like structures in Huh7.5 and C6/36 cells.**

723 MAYV on intercellular extensions: Huh7.5 (upper panel) and C6/36 (lower panel) cells
724 were infected with MAYV, incubated at 37°C for 12 h for Huh7.5 and 24h for C6/36
725 cells, and fixed. Cells were permeabilized and stained for viral E2 envelope protein
726 (green) and phalloidin to detect F-actin (red) and nucleus (blue) with Hoechst stain.
727 Images from one optical section are shown and are representative of three independent
728 experiments.

729 **Figure 5. Macropinocytosis as an additional entry mechanism for MAYV in**
730 **vertebrate hosts.**

731 A) Macropinocytic membrane projections chasing virus particles. Huh7.5, BHK-21 and
732 C6/36 cells infected with MAYV at 5 MOI; 3hpi cells were harvested, processed,
733 sectioned and scanned under TEM. B) MAYV enhances FITC-dextran uptake in
734 vertebrate cells but not mosquito cells. BHK-21, Huh7.5, C6/36 cells were pre-treated
735 with MAYV (lower panel) at MOI of 1 or mock infected for one hour. Cells were then
736 washed and incubated with medium containing FITC-labeled dextran 10,000 MW (1
737 mg/ml). After 20 minutes, cells were washed, fixed and imaged. C) EIPA,
738 macropinocytosis inhibitor inhibits infection of MAYV in vertebrate cells but not mosquito
739 cells. Vertebrate and invertebrate cells were pre-treated with the different
740 concentrations of EIPA, followed by incubation with MAYV at MOI of 0.1 in the
741 continued presence of the drug. Control cells received DMSO instead of the drug. Cells
742 were washed and fixed and probed with appropriate primary and secondary antibodies
743 after 12hpi for vertebrate cells and 24hpi for invertebrate cells. Percent virus infection
744 was calculated and plotted as bar diagram.

745

746 **Figure 6. Electron microscopy analysis of MAYV lifecycle in vertebrate cells.**

747 A) Huh7.5 cells infected with MAYV at an MOI of 5, fixed and sectioned for TEM
748 analysis. Virus entry by (i) clathrin mediated endocytosis pathway and (ii) direct
749 membrane fusion. Cytoplasmic replication spherules with central electron dense
750 structures (iii) and (iv) formation and maturation of nuclear core (NCs) in cytoplasm. v)

751 and vi) release of viral particles by membrane budding and exocytosis. RS=Replication
752 Spherules; CPV: Cytopathic Vacuoles.

753

754 **Figure 7. Electron microscopy analysis of MAYV lifecycle in invertebrate cells.**

755 C6/36 cells were infected with MAYV at an MOI of 5 and fixed for TEM analysis. i) Virus
756 entry via clathrin coated pits like vesicle. ii) and iii) Virus replication inside the replication
757 spherules in the cytopathic vesicle and on the cell membrane. ii) and vi) Virus
758 replication and maturation in cytopathic vesicle I and II hybrid vesicles. v) formation and
759 maturation of nuclear core (NCs) in cytoplasm. Release of viral particles by vii)
760 membrane budding and viii) exocytosis. RS=Replication Spherules; CPV: Cytopathic
761 Vacuoles

762

763 **Figure 8. Both intrinsic and extrinsic apoptotic pathways are activated during
764 MAYV infection.**

765 A) At 3, 6, 9, 12, 24, 36, and 48hpi Huh7.5 cell viability was measured by neutral red
766 uptake assay. Data from three independent experiments were plotted, error bars
767 indicate standard deviations of the means. B) TEM analysis showing apoptotic bleb and
768 nuclear fragmentation of MAYV infected Huh7.5 cell. C) The cleavage of Caspase 3 at
769 12, 24 and 48hpi and PARP at 3,6,12, 24 and 48hpi by Western blot analysis in the cell
770 lysate of mock and MAYV Huh7.5 cells. Uncropped blots are provided as
771 Supplementary Figure 1. Hoechst 33342 staining of MAYV infected Huh7.5 cells (36hpi)
772 observed under UV light. Arrows (bottom righthand side panel) indicate nuclei that
773 contain condensed chromatin. D) Immunofluorescence detection of Cleaved Caspase 9

774 (intrinsic apoptotic marker), Caspase 8 (extrinsic apoptotic marker) at 36hpi and cleaved
775 caspase 3 in MAYV infected Huh7.5 cells. E) Focus size in Vero cells by MAYV infected
776 Huh7.5 cells treated with apoptosis inhibitor (zVAD-FMK) or vehicle control (DMSO).

Fig1.

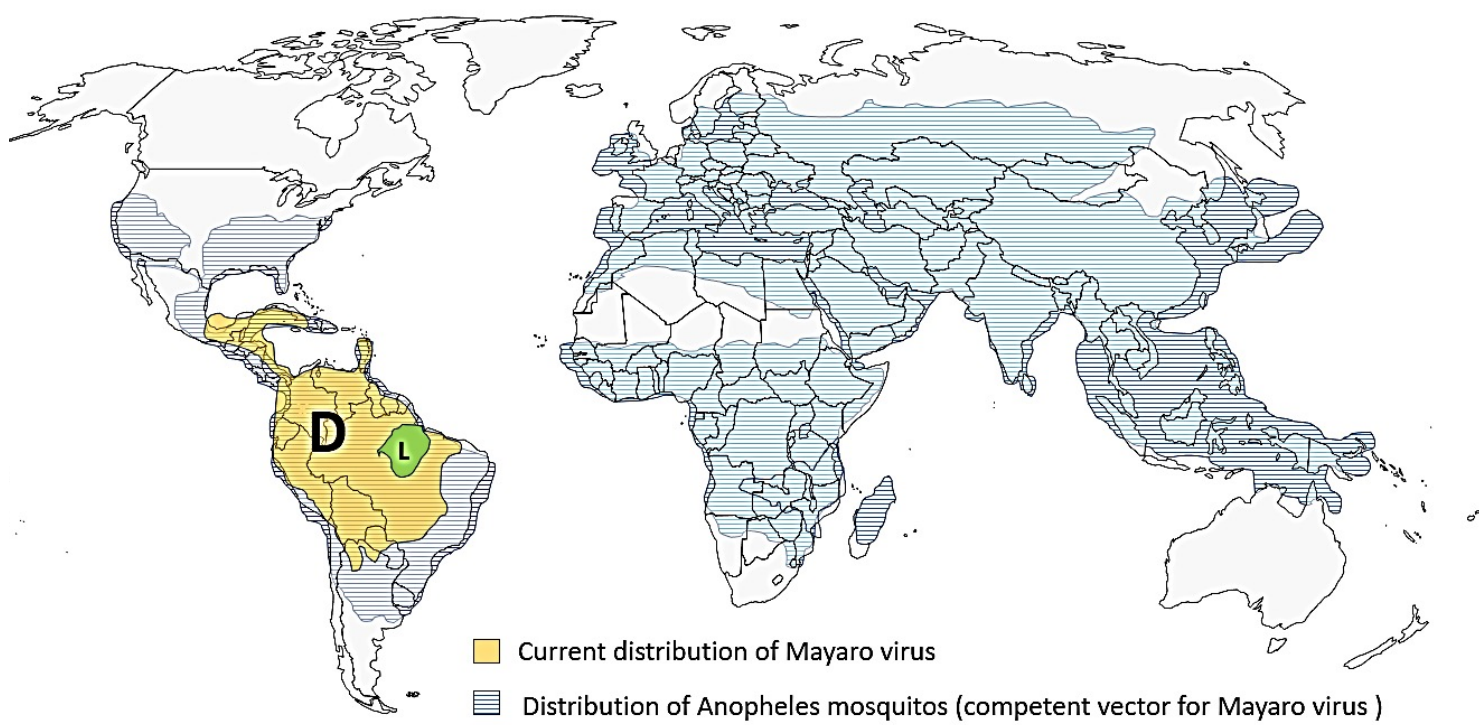


Fig2.

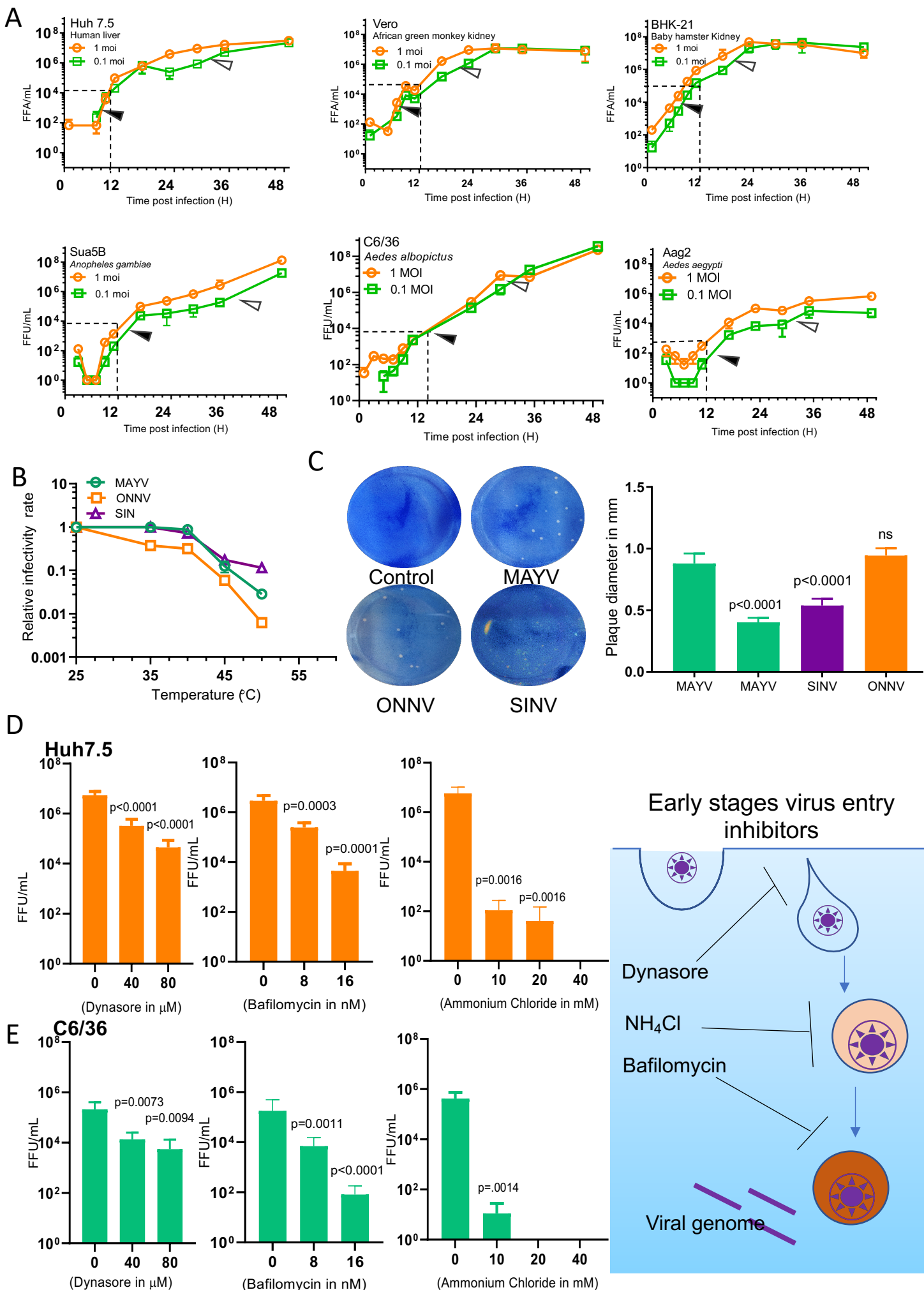
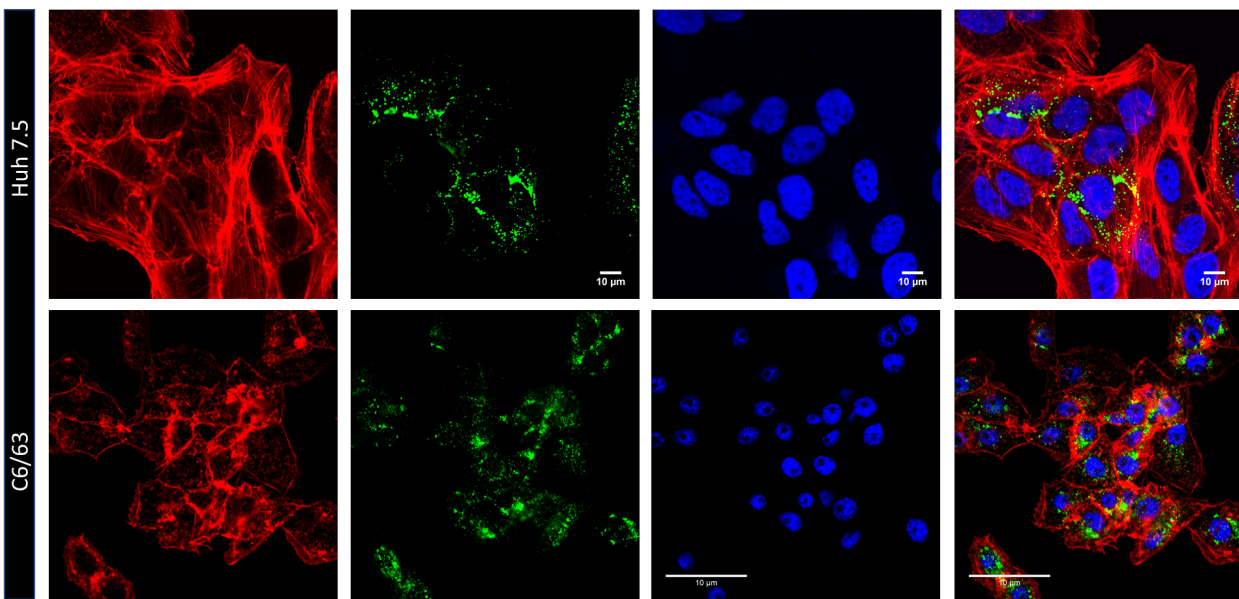


Fig3Phalloidin(β -actin)

dsRNA

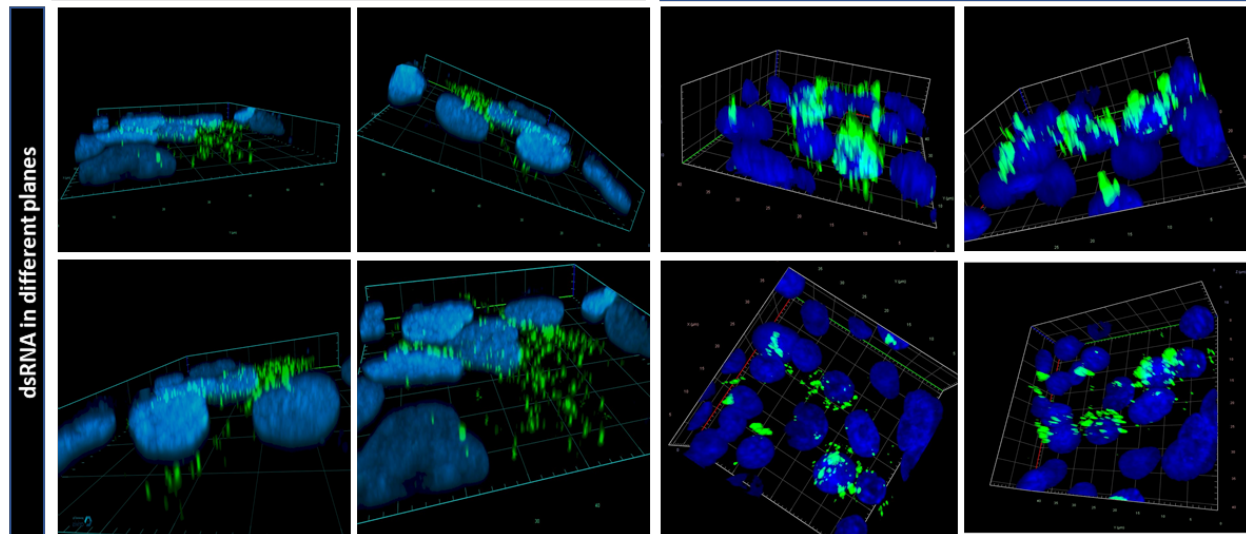
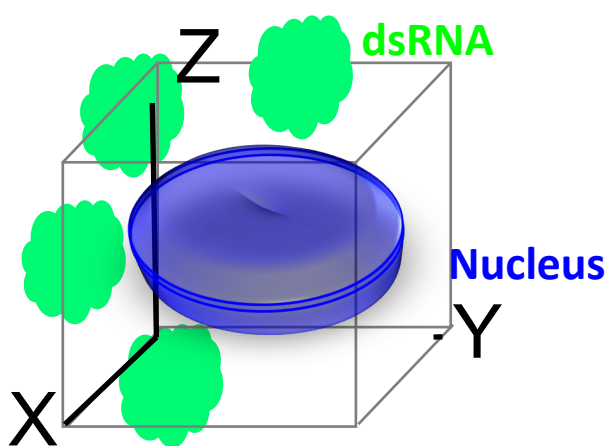
Nucleus(Hoechst)

Merge

A

Huh7.5

C6/36

B**C**

*: Replication spherule
#: Virus particles

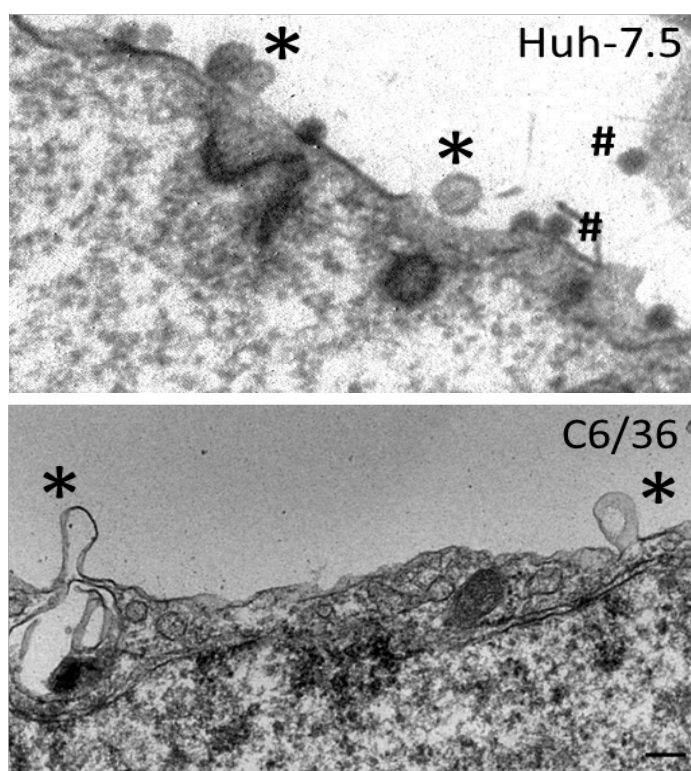
D

Fig4

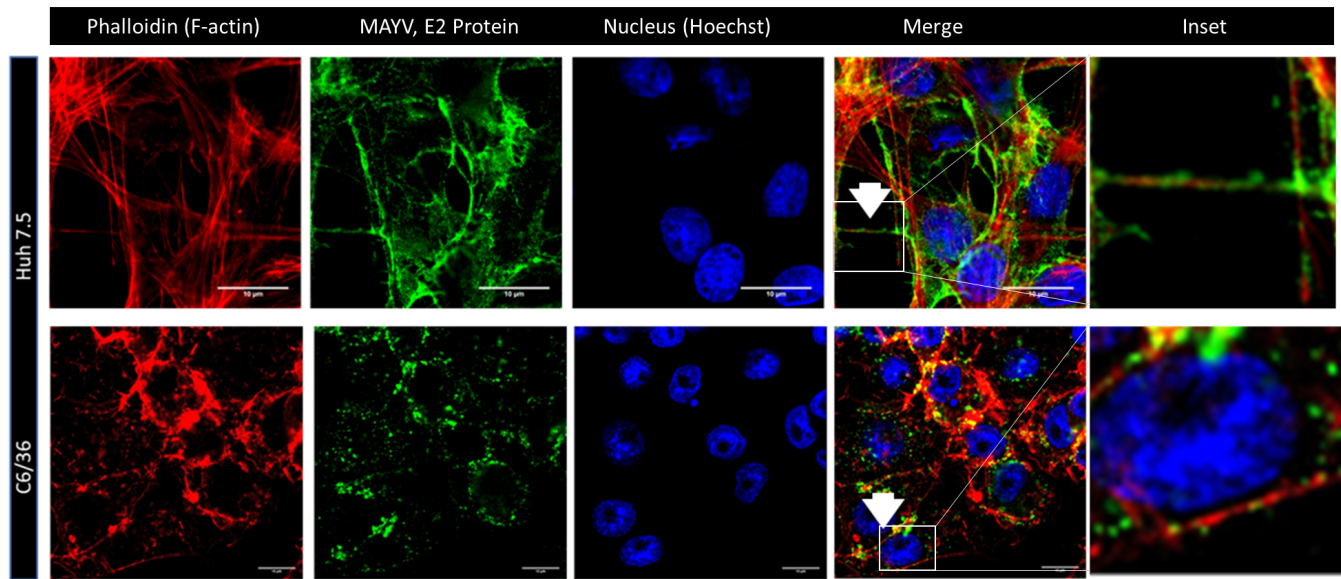
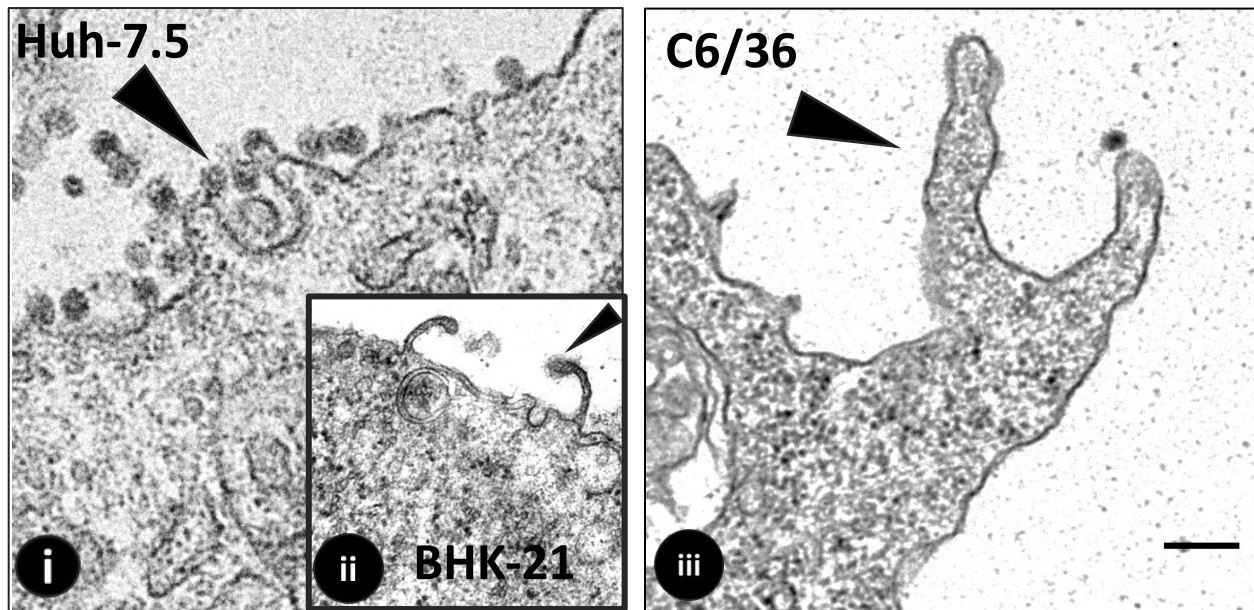


Fig5.

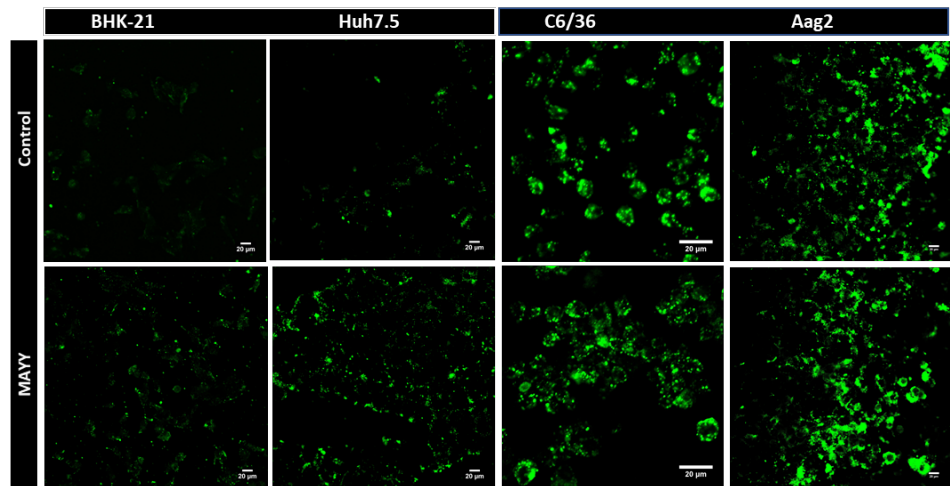
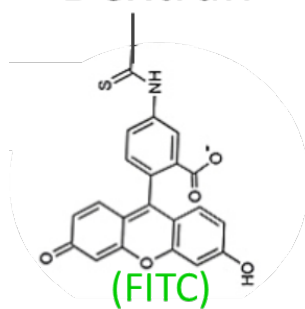
A



B

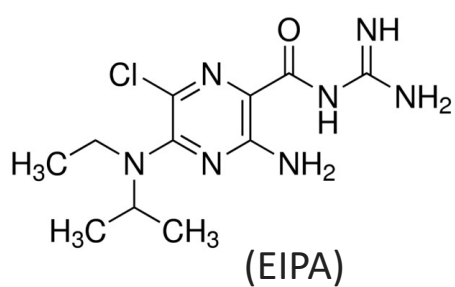
Functional uptake assay

Dextran



C

Pharmacological inhibition assay



Macropinocytosis Blocker

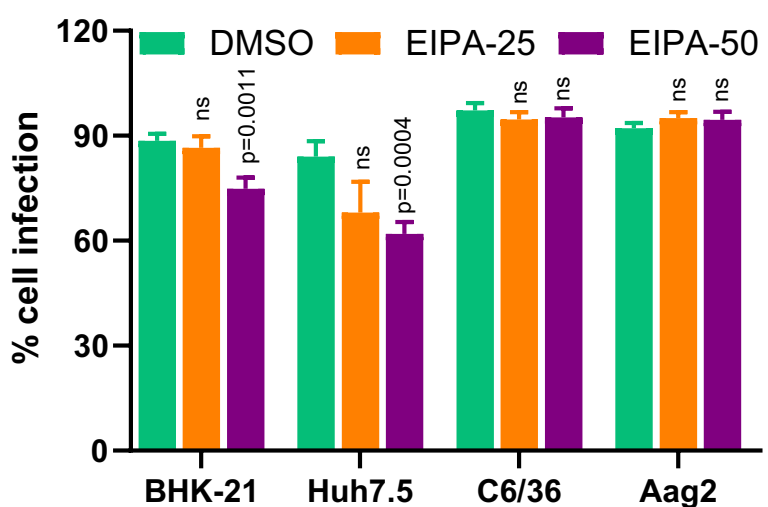


Fig6

Huh7.5 cell

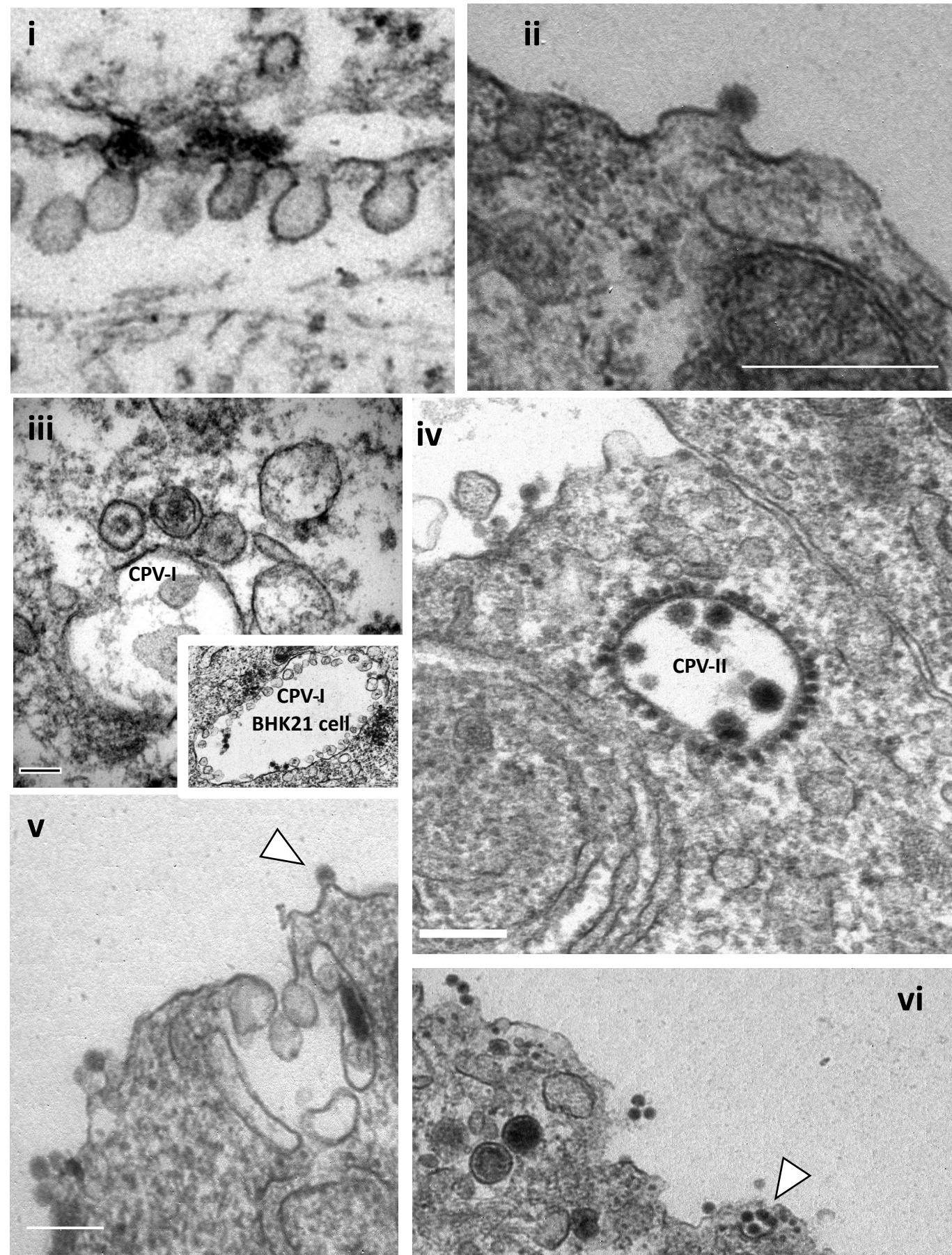


Fig7

C6/36 cell

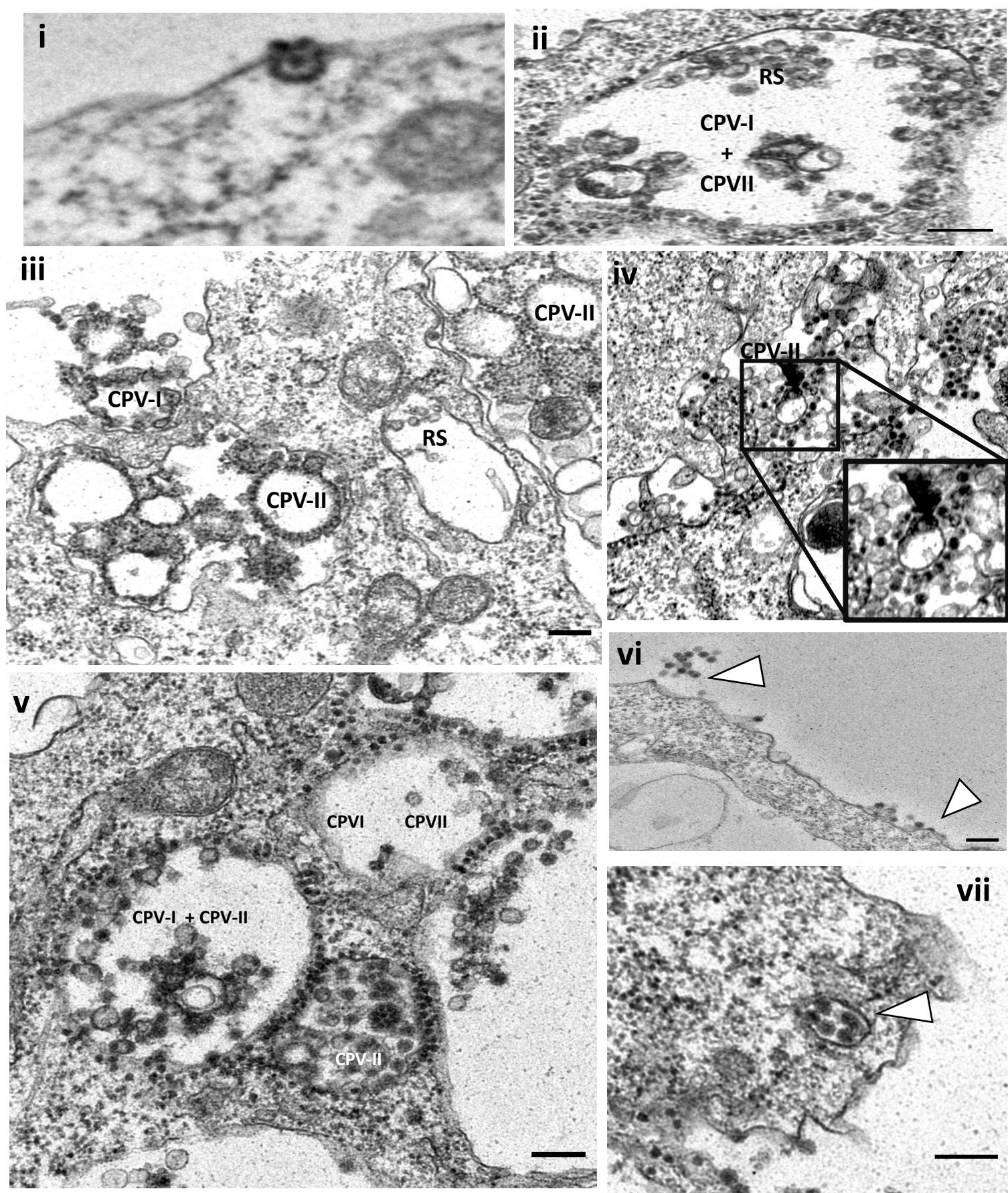
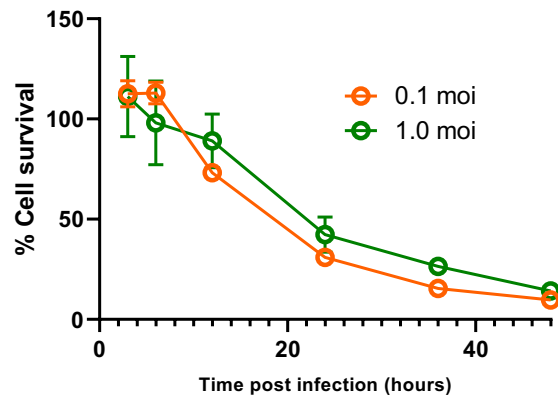
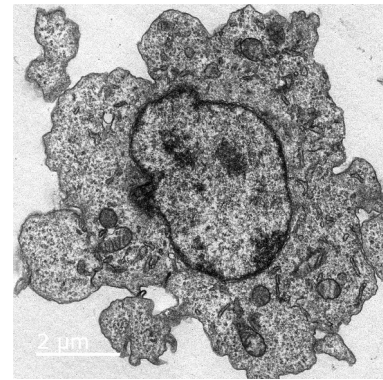
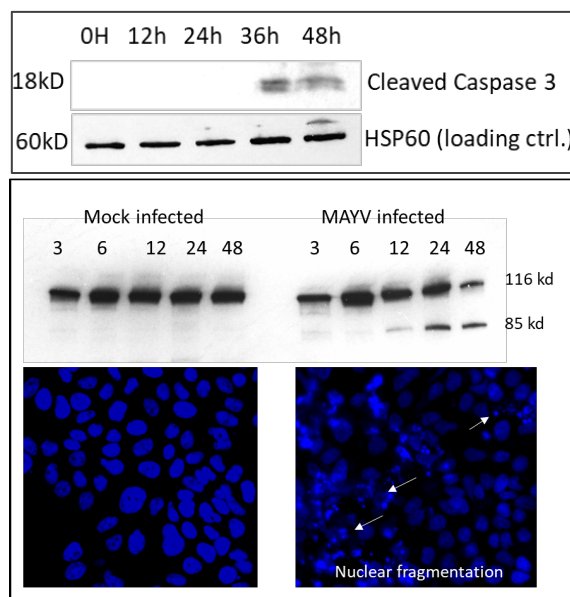
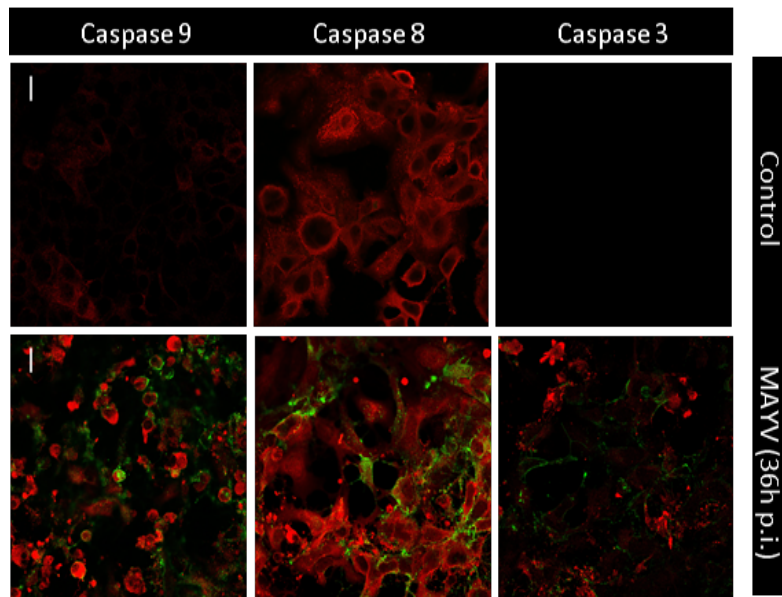


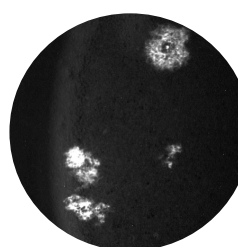
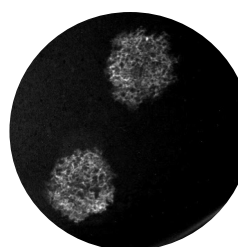
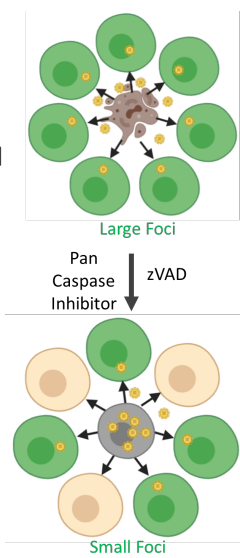
Fig8

**B****C****D****E** Infection of Huh cell

zVAD-FMK DMSO control

Co-culture
Huh cell with Vero cell

Foci size



Focus Diameter
(in arbitrary unit)

